IEEE Access
Multidisciplinary | Rapid Review | Open Access Journal

Received July 27, 2020, accepted August 14, 2020, date of publication August 18, 2020, date of current version August 28, 2020.

Digital Object Identifier 10.1109/ACCESS.2020.3017507

Study of Wind Flow Angle and Velocity on Ice Accretion of Transmission Line Composite Insulators

YAFEI HUANG[1], MUHAMMAD S. VIRK[2], AND XINGLIANG JIANG[1], (Senior Member, IEEE)
[1]State Key Laboratory of Power Transmission Equipment & System Security and New Technology, Chongqing University, Chongqing 400044, China
[2]Arctic Technology & Icing Research Group, University of Tromsø, 8505 Narvik, Norway

Corresponding author: Muhammad S. Virk (muhammad.s.virk@uit.no)

This work was supported by a grant from the Publication Fund of UiT/The Arctic University of Norway.

ABSTRACT Ice accretion on insulators in cold regions is a serious and inevitable problem for power transmission lines, which may cause over-load and icing flashover accidents and can lead to wide power outage. In this research work, multiphase numerical simulations are carried out to investigate the effect of wind flow angle & velocity on the ice accretion of transmission line composite insulators. To verify the simulation results, lab-based icing tests are carried out in artificial climate chamber of Chongqing University. Results show that the change of wind flow angle has an obvious effect on both accreted ice shape and ice mass of insulators. When wind flow angle changes from 0° to 90° or −90°, the ice mass increases before dropping sharply. Meanwhile, ice mass accretion on insulators with wind flow angle is more sensitive to the change of wind velocity. For V-shape insulator strings, the ice mass increased 47.22% in average compared to ordinary suspension insulators. The findings of this research can provide significant engineering reference for the design of transmission line in icing prone areas.

INDEX TERMS Overhead transmission line, CFD, ice accretion, insulator strings, wind flow angle.

I. INTRODUCTION

Icing is a common natural phenomenon in cold regions and poses serious threats to the operations of overhead power transmission lines. Once insulators are covered with ice, transmission lines can face the problems such as discharging, flashover, trip-out and serious widely power outage [1]–[3].

For a long time, plenty of research about insulator icing have been conducted around the world mainly focusing on the icing flashover tests. Based on results of flashover tests, researchers found that ice accretion decreases the flashover voltage of insulators [4]–[6]. Furthermore, the decrease of icing flashover voltage is seriously related to the ice mass and ice shape on insulators [7]–[9]. However, limited work has been carried out in this research field. Rudzinski *et al.* proposed a 3D glaze ice simulation model for post insulator, which is based on discrete particle analysis and takes lots of computation cost [10]. Zhang *et al.* performed icing and flashover test on V-shape insulator stings, and analyzed the ice shape on V-shape insulator stings, but no quantitative measurement was involved [11]. Xingliang *et al.* proposed a calculation method for ice mass estimation on composite insulators, however, in his research, the change of ice shape is not investigated [12]. Jiang *et al.* built a simulation model for glaze ice accretion on insulators, and this model mainly focuses on the formation of icicles [13]. Though several research for ice accretion on insulators have been performed, but ignored the effect of wind flow angle on ice accretion.

It is very common that there is an angle between wind flow and insulators. For some cases, the wind velocity is not horizontal when flows over the vertically installed insulators, and for others the wind is horizontal, but insulators are fixed with an angle due to the use of V-shape insulator stings. Because of the advantages of space saving and stability, V-shape insulator stings is widely used in China, especially in EHV (extra-high voltage) and UEV (ultra-high voltage) transmission line [14], [15]. In the meantime, most of the V-shape insulator stings are consisted of composite insulators due to its excellent mechanical properties and anti-contamination performance [16]. Usually, the selection

The associate editor coordinating the review of this manuscript and approving it for publication was Jenny Mahoney.

of inclination angle of V-shape insulator strings is based on the mechanical properties under the action of wind and based on the statics and dynamics analysis of mechanical performance, the most recommended inclination angle for V-shape insulator strings is between 60° and 120° [17]–[19]. So far, the design of transmission line has not taken into considerations, the effect of the wind flow angle on icing characteristics, which may cause potential problems.

Nowadays, there are three main approaches to study the ice accretion on insulators: field observation, lab-based icing test and numerical simulation method [20]. Compared to field observation and lab-based icing test, numerical simulation method is easy to conduct and save lots of cost in manpower and material resources. However, numerical simulation method needs to be further verified by field observation or artificial icing test.

In this research, CFD based multiphase numerical simulations method is used. Furthermore, the simulation results are verified by icing tests in artificial climate chamber. Then the effect of wind flow angle & velocity on ice accretion of composite insulators is investigated deeply, which provide significant engineering reference for the design of insulators of transmission line in ice prone areas.

II. ICE NUMERICAL SIMULATION MODEL

A. DEFINITION OF WIND FLOW ANGLE

The acute angle between wind velocity and the perpendicular of insulator is defined as wind flow angle α, which is illustrated in Fig. 1. And when wind blow towards the insulator upper surface α is positive, otherwise it is negative. The inclination angle of V-shape insulator strings is β. The α is between $-90°$ and $90°$ and the range of β is 0 - 180°. Furthermore, the relationship between α and β can be expressed as

$$\beta = 2 \cdot |\alpha| \tag{1}$$

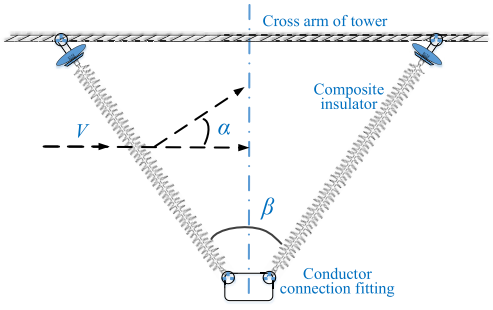

FIGURE 1. Diagram of wind flow angle.

In this research, FXBW-220/100 composite insulators are used. The total length of FXBW-220/100 composite insulators is 2240 mm, and the insulation distance (the length of the insulation part) is 2000 mm with 50 sheds. Because the periodic distribution of big and small insulator sheds, a section containing six sheds is selected as simulation object to save the computational cost. The profile of FXBW-220/100 composite insulator and simulation section are shown in Fig. 2, and the geometric parameters are shown in Table. 1.

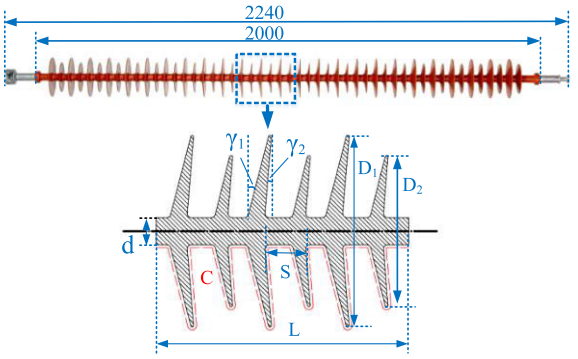

FIGURE 2. FXBW-220/100 composite insulator and simulation selected section.

TABLE 1. Geometric parameters of research object.

L	S	C	d	D_1	D_2	γ_1	γ_2
250	40	79.2	28	188	148	15	5

L is the height of test insulator section (mm); S is the sheds spacing (mm), which means the spacing distance between adjacent sheds; C is creepage distance of test insulator section (mm), which means the shortest distance along the surface of insulator between two ends; d is the rod diameter (mm); D_1, D_2 are lager sheds diameter and small sheds diameter respectively (mm); γ_1 is upper tilt angle (°), which means the acute angle between horizontal plane and shed upper surface; γ_2 is lower tilt angle (°), which means the acute angle between horizontal plane and shed lower surface .

B. NUMERICAL SETUP

In this research, CFD based multiphase numerical simulations are carried out. The simulation domain and mesh are shown in Fig. 3. The domain is composed of velocity-inlet, pressure-outlet, slip wall of around faces and no-slip wall for insulator.

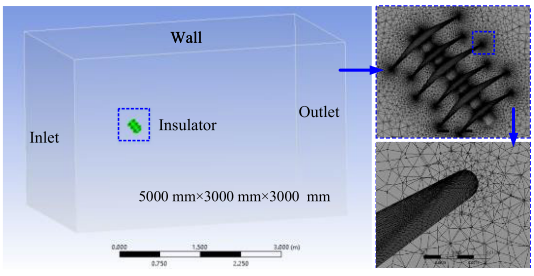

FIGURE 3. Simulation domain and mesh.

To make sure the good simulation of air flow behaviors and heat flux transfer on insulator surface, the mesh size on insulator surface is 10^{-3} m and the first layer height of grids is set to 10^{-6} m with 1.1 growth rate. In average, there are about 2.9 - 3.5 million cells and 0.7 - 0.9 million nodes in simulation domain. In mesh sensitivity analysis, the heat flux transfer and droplet solution on insulator surface are selective

analyzed regarding the independence of the numerical solution from the mesh size. The heat flux and shear stress and, a y+ values of less than 1 is used near the wall surface are accurately determined. At the same time, number of mesh elements and y+ value is selected based upon the heat flux calculations, where a numerical check is carried out that the heat flux computed with the classical formulae *dT/dn* should be comparable with the heat flux computed with the Gresho's method. Results show that the numerical mesh is usable and stable in this research.

The Eulerian two-phase model is used to solve air flow field and water droplets distribution around insulator. Air flow around insulators can be solved by the differential equations of motion of incompressible viscous fluid including continuity equation, momentum conservation equation and energy conservation equation [21], [22]:

$$\partial\rho_a/\partial t + \vec{\nabla}\left(\rho_a\vec{v}_a\right) = 0 \tag{2}$$

$$\partial\rho_a\vec{v}_a/\partial t + \vec{\nabla}\left(\rho_{\mathrm{a}}\vec{v}_a\vec{v}_a\right) = \vec{\nabla}\cdot\sigma^{\mathrm{ij}} + \rho_a\vec{g} \tag{3}$$

$$\partial\rho_{\mathrm{a}}E_a/\partial t + \vec{\nabla}\left(\rho_{\mathrm{a}}\vec{v}_aH_a\right) = \vec{\nabla}\cdot\left(\kappa_{\mathrm{a}}\left(\vec{\nabla}T_a\right) + \upsilon_i\tau^{ij}\right) + \rho_{\mathrm{a}}\vec{g}\cdot\vec{v}_a \tag{4}$$

where ρ_a is the air density; $\boldsymbol{v_a}$ is the air velocity vector; σ^{ij} is the stress tensor; E_a is the total energy; H_a is the total enthalpy; T_a is the air static temperature; κ_a is the air thermal conductivity.

In this research, K-ω SST turbulence model is used to solve the air flow around insulator. Meanwhile, Sand-Grain model is used to simulate the ice surface roughness. For water droplets, Eulerian model is used in which water droplets are viewed as continues phase. The distribution of water droplets is calculated by solving continuity equation and momentum conservation equation [22]–[24]:

$$\partial\alpha_d/\partial t + \vec{\nabla}\left(\alpha\vec{v}_d\right) = 0 \tag{5}$$

$$C_DRe_d\alpha_d\left(\vec{v}_a - \vec{v}_d\right)/24K + \alpha_d\left(1 - \rho_a/\rho_d\right)/Fr^2 = \partial\left(\alpha_d\vec{v}_d\right)/\partial t + \vec{\nabla}\left[\alpha_d\vec{v}_d\otimes\vec{v}_d\right] \tag{6}$$

where α_d is the water volume fraction; $\boldsymbol{v_d}$ is the velocity of droplet; ρ_d is the droplets density; C_D is the droplet drag coefficient; Re_d is the Reynolds number of droplets; K is inertial parameter: Fr is the local Froude number.

$$Re_d = \rho_aR_dV_\infty\left\|\vec{v}_a - \vec{v}_d\right\|/\mu_a \tag{7}$$

$$K = \rho_dR_d^2v_\infty/18L_\infty\mu_a \tag{8}$$

$$Fr = \|v_\infty\|/\sqrt{L_\infty g_\infty} \tag{9}$$

where R_d is droplet diameter; v_∞ is initial air flow velocity; μ_α is air kinematic viscosity; L_∞ is the characteristics length of object; g_∞ is acceleration of gravity.

After getting the distribution of water droplets around insulator, the collision efficiency of water droplets on insulator is calculated. To solve the droplets freezing process on insulator surface, mass and energy conservation equations are used [22]–[25]:

$$\rho_f\left[\partial h_f/\partial t + \vec{\nabla}\left(\vec{v}_fh_f\right)\right] = v_\infty\omega_d\beta_d - m_{evap} - m_{ice} \tag{10}$$

$$c_fT_fm_{film} + L_{evap}m_{evap} + c_h\left(T_{\mathrm{f}} - T_{ice}\right) + q_{cond} = \left(L_{fusion} - c_sT\right)m_{ice} + \sigma\varepsilon\left(T_\infty^4 - T_f^4\right) + \left(c_f\left(T_\infty - T_f\right) + \|\vec{v}_d\|^2/2\right)m_{imp} \tag{11}$$

where ρ_f, h_f, $\boldsymbol{v_f}$, c_f are parameters of water film, which are density, height, velocity vector, and specific heat capacity of water film respectively; ω_d is the liquid water content; β_d is the collision efficiency; m_{evap} is the mass transfer by evaporation; m_{ice} is the mass transfer by ice formation; T_f is the environmental temperature; T_∞ is the initial temperature of air; L_{evap} is evaporation latent heat; L_{fusion} is fusion latent heat; c_s is the specific heat capacity of ice; T is the freezing temperature; σ is the Stefan constant; ε is the emissivity of the ice surface; c_h is the convective heat transfer coefficient; T_{ice} is the ice temperature of ice surface; q_{cond} is the conductive heat fluxes.

In this research, airflow and droplet solvers are based on Finite Element base discretization method, but ice accretion solver is based on Finite volume base discretization method. By solving (2) - (11), the ice mass accreted on every control volume (grid) on insulator surface is achieved. After the calculation of ice density, the ice volume on every grid is also obtained. Then the ice shape on insulator surface can be worked out by grid transformation and reorganization.

III. ICING TEST AND MODEL VALIDATION

A. TEST FACILITIES, SPECIMENS AND PROCEDURES

To verify the numerical simulation results, icing tests of FXBW-220/100 composite insulator are carried out in the artificial climate chamber of Chongqing University, which is shown in Fig. 4. With a diameter of 7.8 m and a height of 11.6 m, the artificial climate chamber of Chongqing University is able to simulate various complex icing environments [12]. The temperature of the climate chamber can be lowered to − 45 ° by refrigeration system. The wind speed can be adjusted between 1 - 12 m/s by wind circulation system. Spaying system are made of IEC standard nozzles and MVD (droplets Median Volume Diameter) can be controlled between 20 μm and 200 μm. Test performance of artificial climate chamber meets the IEEE icing experiment standards [26], [27].

-Icing test procedure. First of all, the insulator is cleaned and dried. Before icing test, insulator is fixed in the climate chamber with a desired angle. Freezing water is pre-cooled to about 1 ° before sent to spraying system. In the icing test, refrigeration system is turned on firstly. When temperature in climate chamber reached to the desired value, wind circulation system and spaying system start working. In icing test, wind generated by wind circulation system is adjusted to move horizontally and brings droplets moving horizontally. In the meantime, spray system is adjusted to generate the

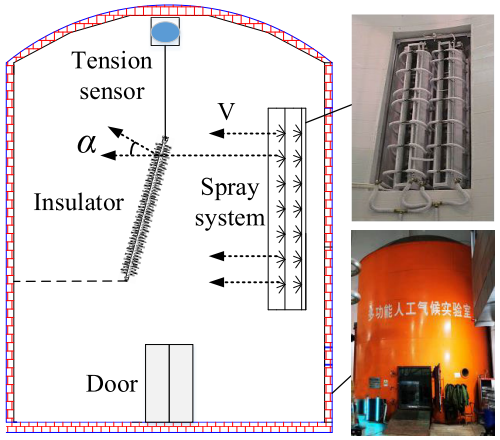

FIGURE 4. Artificial climate chamber.

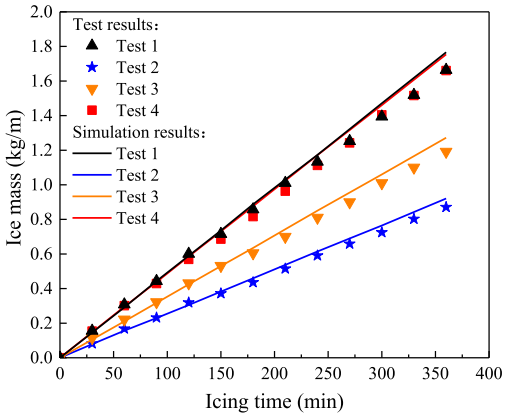

FIGURE 5. Ice mass increasing with time in test and simulation results.

required size of the water droplets and water content to meet. the experimental requirement. Detailed icing test procedures strictly follow the instruction in IEEE. 1783 Guide [27].

-Measurement of Ice mass. Test insulator is hung in artificial climate chamber by the way of tension sensor (DEG-50 kg with ± 0.02% measure error). Subtracting the original weight of the insulator and other fittings from the reading of the tension sensor is the ice mass accretion on insulator. Every icing test last 360 min and ice mass is recorded after every 30 min. Four icing tests are carried out, and the parameters of icing test are shown in Table. 2.

TABLE 2. Parameters of icing test.

Parameters	*V*	*T*	*LWC*	*MVD*	*α*
Test 1	9	-3	0.6	25	0
Test 2	6	-3	0.6	25	0
Test 3	6	-3	0.6	25	40
Test 4	6	-3	0.6	25	-40

V is wind velocity (m/s); *α* is wind flow angle (°); *T* is temperature (°C); *LWC* is liquid water content (g/m^3); *MVD* is droplets median volume diameter (μm).

B. TEST RESULTS

Ice mass accretion on insulators increases with time in both test and simulation results are shown in Fig. 5. The ice mass accreted on insulators is converted to per meter. Fig. 5 shows the following:

1) The ice mass increases quasi-linearly with icing time in both test and simulation results with saturation tendency. Although there is acceptable difference, the simulation results are closed to the test results.
2) Although there are fluctuations in the percentage difference in ice mass between test and simulation results in the early stage of the icing test, but as the experiments progress, it gradually stabilizes. The reasons could be the effect of insulator surface material. Composite insulators are made of hydrophobic silicone rubber, which designed for anti-contamination performance. In early stage of the icing test, water on insulator surface is easy to condense into drops and freeze, resulting in the increased roughness of the insulator surface and lead to more ice accreting. As test progressing, when the insulator surface is covered with ice, the ice accretion is no longer affected by the surface material. So, the difference between test and simulation results gradually become stable.
3) It can be found that the change of wind velocity has obvious impact on the ice accretion. When wind velocity increase from 6 m/s to 9 m/s, the ice mass almost doubles which augments from 0.871kg/m to 1.671kg/m at 360 min in test result.
4) In the meantime, wind flow angle also has great effect on the ice accretion of insulators. It can be found that the ice mass increase obviously when wind flow angle changing from 0° to 40 ° or −40°. Comparing the test results in test 2, test 3 and test 4, with the same environmental parameters, the ice mass are 0.871 kg/m, 1.192 kg/m, and 1.664kg/m at 360 min respectively.

The percentage difference and RMSE (root mean square error) between test and simulation results are shown in Table. 3. The RMSE between test and simulation results in 4 tests are all less than 0.05 kg/m, and the total difference between test and simulation results is 5.65%. In summary, the ice simulation model performs well in calculation of ice mass accreted on insulators. Though with acceptable difference, ice simulation method is more efficient and low-cost compared to the field observation and lab-based icing test.

TABLE 3. Percentage difference and RMSE between test and simulation results.

	Test 1	Test 2	Test 3	Test 4
Difference	4.96%	6.18%	5.91%	5.57%
RMSE (kg/m)	0.0269	0.0433	0.0418	0.0480

IV. EFFECT OF WIND FLOW ANGLE ON ICE SHAPE

In this section, the most common value of *α* in practice (0° and ± 40°) are selected to investigate the effect of wind

flow angle on air flow behaviors, droplets collision efficiency, ice shape and ice thickness on insulator surface. The simulation parameters in this section are shown in Table. 4. Simulation time is 360 minutes.

TABLE 4. Simulation parameters.

T (°C)	V (m/s)	LWC (g/m^3)	MVD (μm)
-3	6	0.6	25

A. AIR FLOW BEHAVIORS

The air flow behaviors at $\alpha = 0°$ and $\alpha = \pm 40°$ cases are illustrated respectively in Fig. 6, and the following can be inferred:

1) Because of the disturbing effect of insulator on air flow field, the wind velocity on windward side is small than the initial value. Besides, the wind velocity along insulator leeward side is almost zero.
2) The largest wind velocity in center section at $\alpha = 0°$ case appears on the rod edge, which is 9.22 m/s. Meanwhile, when $\alpha = 40°$ and $\alpha = -40°$, The largest wind velocity appears on the edge of insulator shed, which are 9.60 m/s and 9.82 m/s respectively. This is because the existing of wind flow angle increases blocking effect of insulator sheds on air flow, and the largest wind velocity usually appears on the edge of blocking object.
3) The wind velocity at different parts of the insulator varies greatly, which has great effect on the transform of heat flux and then water droplets freezing process.
4) The distribution and flow field of water droplets depends on the air flow behaviors. Some water droplets will bump onto the insulator surface and others will go around the insulator with air. To investigate the collection characteristics of water droplets on insulator surface, the droplets collision efficiency is calculated.

B. DROPLETS COLLISION EFFICIENCY

The droplets collision efficiency is a significant parameter for the icing simulation, which reveal how much water droplets will get onto to the insulator surface and participate in the freezing process. Usually, larger droplets collision efficiency means more ice accretion. So, through the distribution of water droplets, where the ice will accrete a lot can be inferred roughly.

The droplets collision efficiency at different cases is shown respectively in Fig. 7. Following are the main observations:

1) When $\alpha = 0°$, the droplets mainly collide onto insulator rods and shed surfaces along windward side. Furthermore, the greatest value for droplets collision efficiency is 0.662, which appears on the insulator rod center.
2) As for $\alpha = 40°$, the droplets collision efficiency in small shed edges and the upper half of the rods are much bigger than other areas, and the biggest droplets

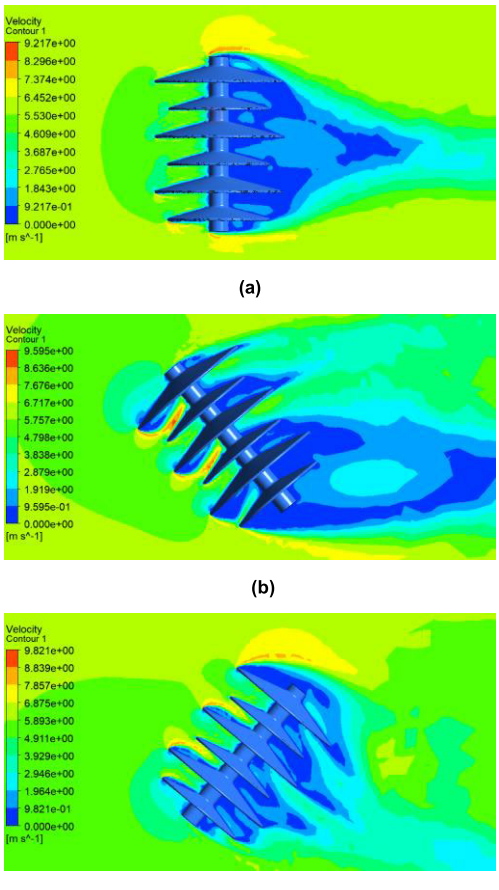

FIGURE 6. Velocity contour along insulator at different angles (center section): (a) $\alpha = 0°$, (b) $\alpha = 40°$, (c) $\alpha = -40°$.

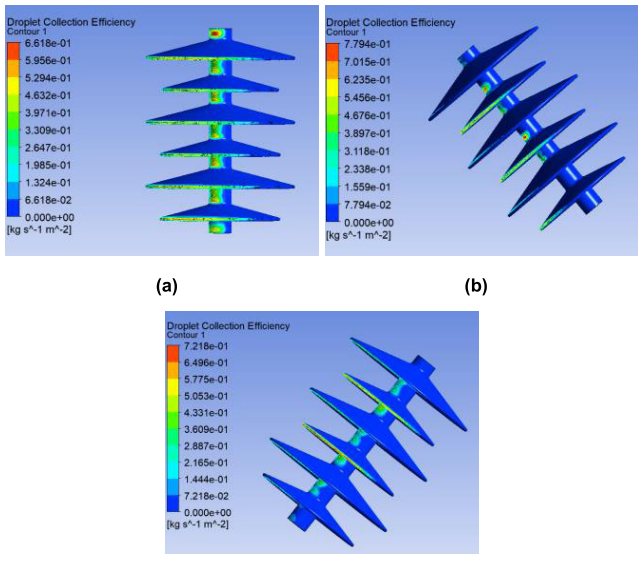

FIGURE 7. Diagram of droplets distribution: (a) $\alpha = 0°$, (b) $\alpha = 40°$, (c) $\alpha = -40°$.

collision efficiency appears on the second small shed edge with 0.779.

3) When it comes to $\alpha = -40°$, it is found is that the droplets mainly collide onto small shed edges and the lower half of the rods. The largest collision efficiency appears in the fourth small shed edge with 0.722.
4) On the leeward the droplets collision efficiency is very small. Because it is difficult for water droplets to get into this area with air flow.
5) It can be found that the wind angle obviously changes the distribution of droplets collision efficiency, which will also greatly influence the accreted ice shape on insulator.

C. ACCRETED ICE SHAPE

The distribution of ice shape in three cases is shown in Fig. 8. It is found that the distribution of ice shape is mainly consistent with the distribution of collision efficiency, as area where with the lager droplets collision efficiency is covered with thick ice. When $\alpha = 0°$, the ice mainly accreted on the insulator rods and shed surfaces. And when $\alpha = 40°$, the ice mainly accreted on the top half of the insulator rods and upper surface beside shed edges. Meanwhile, at $\alpha = -40°$ case, ice mainly appears on the lower half of the insulator rods and lower surface beside shed edges. It is also notable that there is also a small amount of ice accreted on the leeward side of insulators. This is because a small amount of water droplets will also follow the eddy currents on insulator leeward side get onto the insulator surface.

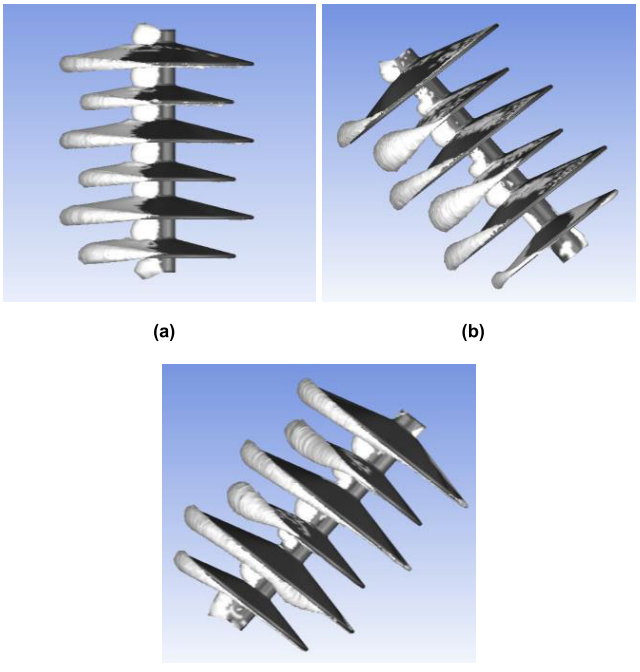

FIGURE 8. Distribution of ice shape: (a) $\alpha = 0°$, (b) $\alpha = 40°$, (c) $\alpha = -40°$.

D. ICE THICKNESS

The distribution of ice accretion can be illustrated further by the analysis of ice thickness. In Fig 9, ice thickness along windward center cross section changing with icing time is shown. When $\alpha = 0°$, the largest ice thickness is 17.04 mm, which appears on second rod. And when $\alpha = 40°$, the largest ice thickness is 21.19 mm which is on upper surface beside the second shed. At the same time, when $\alpha = -40°$, the largest ice thickness is 17.18 mm which appears in lower

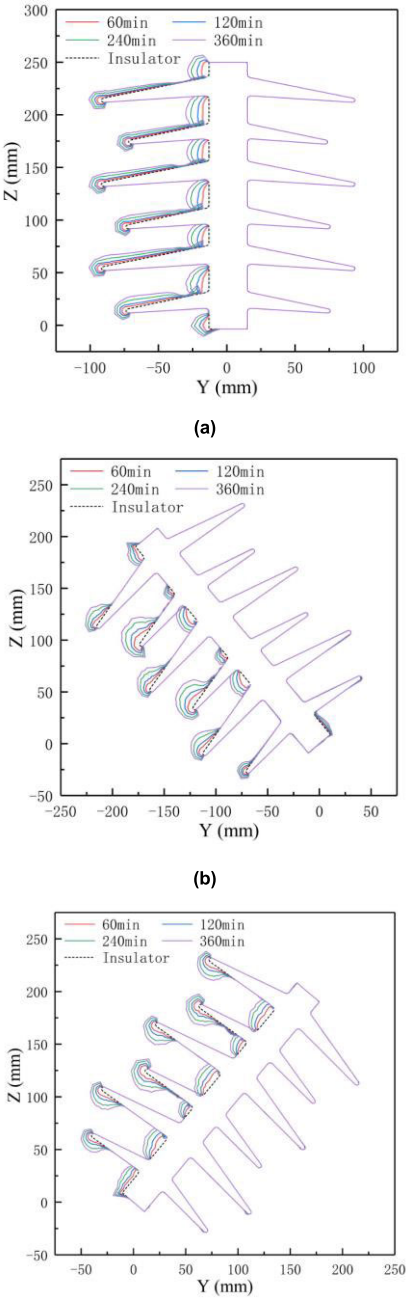

FIGURE 9. Ice thickness changing with time: (a) $\alpha = 0°$, (b) $\alpha = 40°$, (c) $\alpha = -40°$.

surface beside the fourth shed. It is obvious that the wind angle greatly changes the distribution of ice on insulator surface. Based on the above research, the existing wind angle obviously changes the air flow behaviors around the insulator. As a result, the distribution of droplets collision efficiency on insulators also totally changes, which further leads to the difference in ice shape on insulators.

V. EFFECT OF WIND FLOW ANGLE ON ICE MASS

In this section, the α (wind flow angle) is changed from $-90°$ to $90°$ to investigate the effect of wind flow angle on the accreted ice mass. Furthermore, the ice mass on V-shape insulator strings with different β (inclination angle) is also studied.

A. WIND FLOW ANGLE BETWEEN 0° AND 90°

As shown in Fig. 10(a), with the increase of icing time, the ice mass of different cases arguments with different rate. To show the difference more clearly, the ice mass for all cases in 360 min are displayed in Fig.10(b). It is found that when α changes from 0° to 90°, the ice mass increases firstly and then drop. The biggest value for ice mass appears at 30° case, which is up to 1.54 kg/m.

There are several reasons for why ice mass changes with wind flow angle and where the maximum value occurs. Firstly, as analyzed in section IV, the change of wind flow angle will greatly influence the air flow behaviors around insulators. The wind velocity at different parts of the insulator varies greatly, which will influence the heat flux transfer and water freezing process. Secondly, the change of wind flow angle will greatly influence the distribution of droplets collision efficiency, which have effect on ice shape and ice mass directly. Thirdly, due to the existence of the wind flow angle, the ice-covered area of insulators changed significantly. According to above research, ice mainly accreted on the windward side, and with the change of wind flow angle, the total windward area of insulator become smaller. This is also a significant reason for the change of ice mass.

B. WIND FLOW ANGLE BETWEEN −90° AND 0°

The ice mass changing with time when α between $-90°$ and $0°$ is illustrated in Fig. 11(a), and the difference in ice mass between cases in 360 min is shown in Fig. 11(b). Similarly,

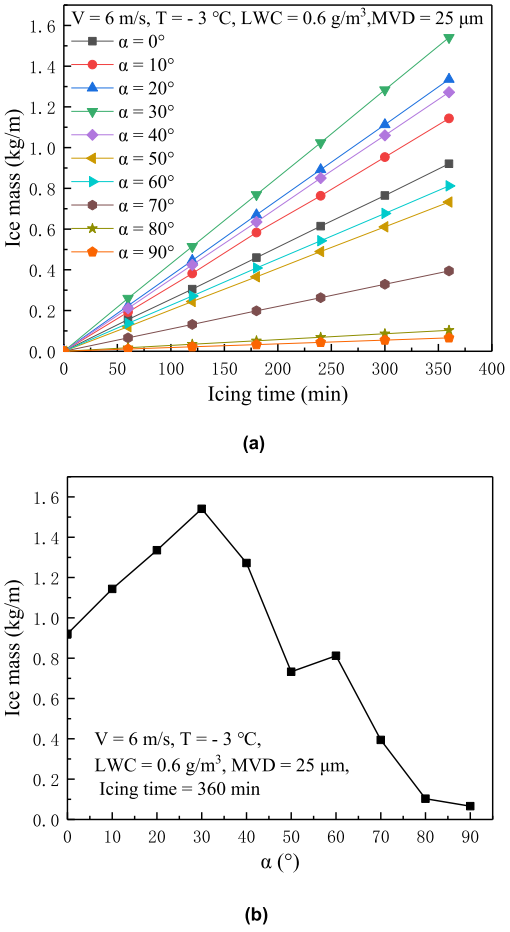

FIGURE 10. Ice mass changing with α (α between 0° and 90°): (a) ice mass changing with time, (b) ice mass at 360 min.

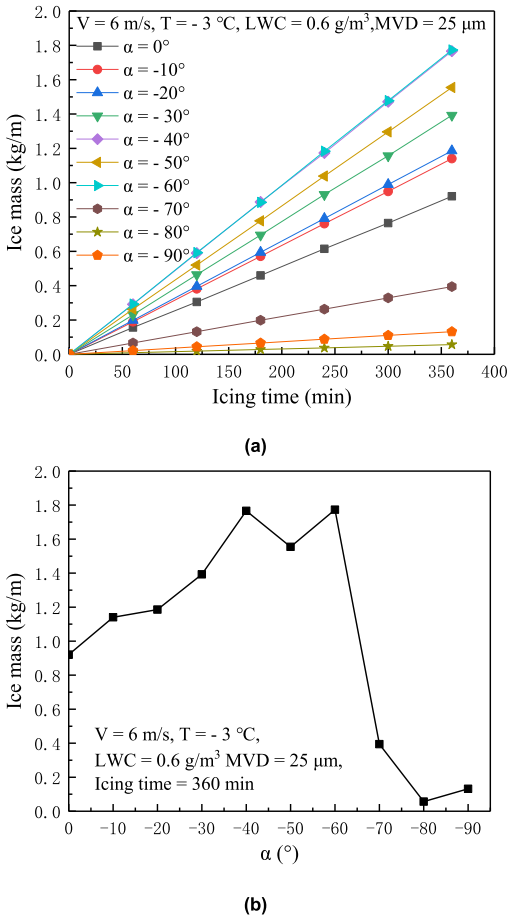

FIGURE 11. Ice mass changing with α (α between 0° and −90°): (a) ice mass changing with time, (b) ice mass at 360 min.

the ice mass mainly increases firstly and then drops when α changing from 0° to −90°. It is worth noting that there is a fluctuation when α changing from −40° to 60° and the largest ice mass appears in −60° case with 1.77 kg/m.

C. INCLINATION ANGLE BETWEEN 0° AND 180°

Generally, a V-shape insulator can be regarded as the combination of two single insulators with different wind flow angle. Furthermore, the ice mass on V-shape insulator surface equals to the sum of ice mass on two single insulators with different wind flow angle. The change of ice mass on V-shape insulator string with different β is shown in Fig. 12(a), and the ice mass on different V-shape insulator strings at 360 min is shown in Fig. 12(b). It can be found that when β changes from 0° to 180°, the ice mass decreases after a firstly increase.

Percentage increase of ice mass on V-shape insulator string compared with ordinary suspension insulators ($\beta = 0°$) is shown in Table. 5. It is notable that when inclination angle is between 60° - 120° (most common value for β), the ice mass increases obviously compared to ordinary suspension insulator strings. When $\beta = 80°$, the ice mass increases 64.99%, and for average, the ice mass increase 47.22%. So, it is significant to take the effect of wind flow angle into consideration when designing insulator strings. Otherwise,

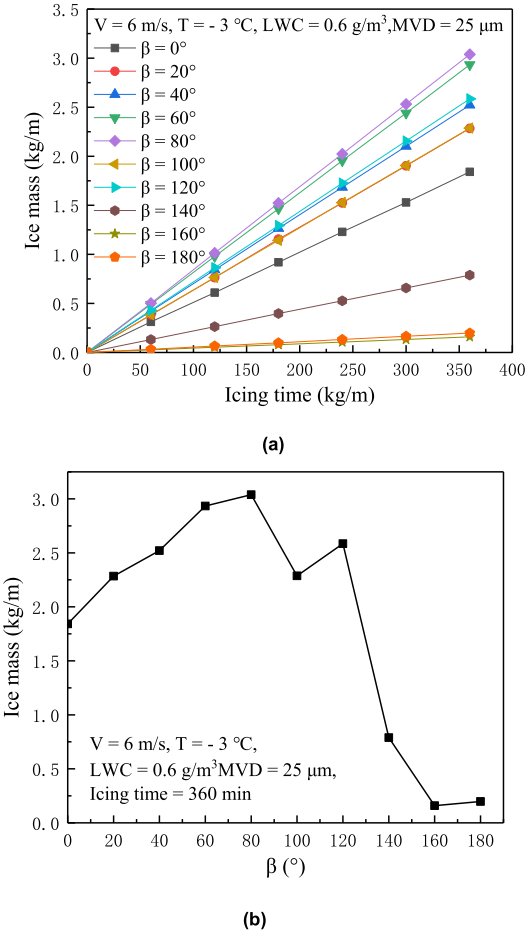

FIGURE 12. Ice mass changing with β: (a) ice mass changing with time, (b) ice mass at 360 min.

TABLE 5. Percentage increase of ice mass.

β (°)	60	80	100	120	Average
Percentage increase	59.30%	64.99%	24.20%	40.38%	47.22%

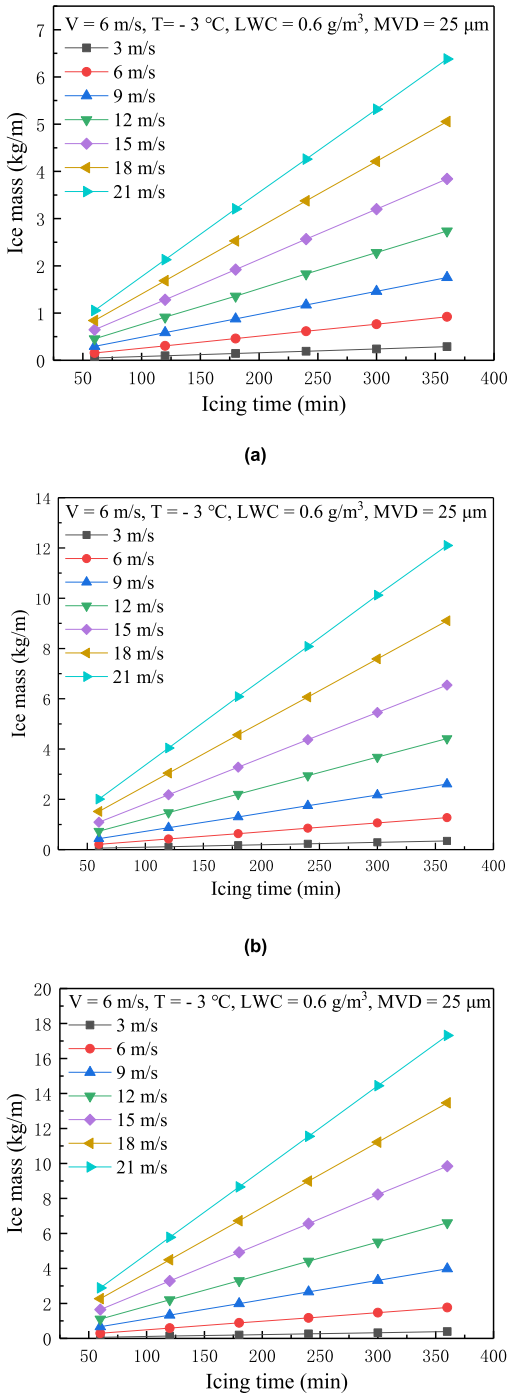

FIGURE 13. Ice mass changing with time under different wind velocity: (a) $\alpha = 0°$, (b) $\alpha = 40°$, (c) $\alpha = -40°$.

the transmission line will face the problem of over-load and icing flashover due to wrong prediction of ice mass.

VI. EFFECT OF WIND VELOCITY ON ICE MASS

In this section, the cases of $\alpha = 0°$ and $\alpha = \pm 40°$ were selected to further study the effect of wind flow angle & velocity on ice mass.

A. ICE MASS CHANGING WITH WIND VELOCITY

The situation of ice mass changing with icing time under different wind velocity are shown in Fig. 13. It can be found that the ice mass on insulator increases with icing time. Furthermore, for both $\alpha = 0°$ and $\alpha = \pm 40°$, the increase rate of ice mass ascends evidently with the argument of wind velocity.

B. SENSITIVITY OF ICE MASS TO WIND VELOCITY

The ice mass with different wind velocity at 360 min is shown in Fig. 14. It is found that when $\alpha = \pm 40°$ the ice mass is always much larger than $\alpha = 0°$ case, which means that insulator strings with $\pm 40°$ wind flow angle are prone to ice disaster because they will get more ice mass in same time span.

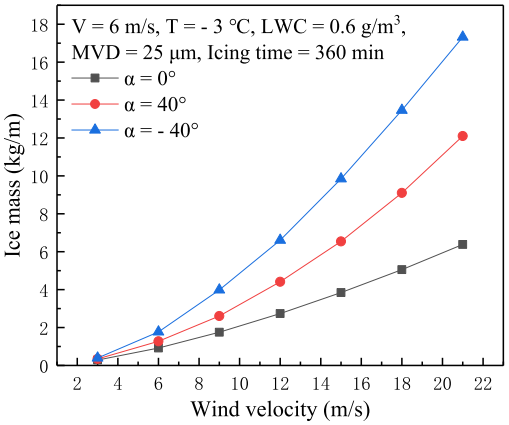

FIGURE 14. Effect of wind velocity on ice mass.

To illustrate the sensitivity of ice mass to wind velocity, sensitivity parameter k_m is defined as:

$$k_m = \Delta m / \Delta V \tag{12}$$

where: Δm is the difference value of icing mass in kg/m (In this research the icing time for Δm *is* 360 minutes); ΔV is the difference value of wind velocity in m/s.

The k_m in different time periods of three cases are shown in Table. 6. For all α, the k_m augments faster and faster with the increase of wind velocity. Furthermore, in $\alpha = 0°$, $\alpha = 40°$, and $\alpha = -40°$ cases, the average value of k_m are 0.304, 0.576, and 0.825 respectively. It can be inferred that when $\alpha = \pm 40°$, the ice mass is much more sensitive to the increase of wind velocity, especially when α is negative. To be specific, when wind velocity increases, the increase rate of ice mass for insulator strings with $\pm 40°$ wind flow angle become more and more lager than ordinary suspension insulator strings. However, this characteristic is always overlooked in the design of transmission lines, which may cause icing disasters when extreme environment (cold current and high wind) comes.

TABLE 6. The values of sensitivity parameter.

Wind velocity (m/s)	$\alpha = 0°$	$\alpha = 40°$	$\alpha = -40°$
0-3	0.096	0.116	0.13
3-6	0.211	0.308	0.459
6-9	0.278	0.445	0.738
9-12	0.328	0.603	0.876
12-15	0.368	0.709	1.079
15-18	0.405	0.853	1.207
18-21	0.441	0.999	1.285
Average	0.304	0.576	0.825

VII. CONCLUSION

Following are the main findings of this research work.

1) Numerical simulation method performs well in ice mass calculation. Compared with the experiment results, the average difference in ice mass is 4.96%-6.18%.
2) The change of wind flow angle has an evident effect on the ice accretion of insulators both in ice shape and ice mass. For single insulator, when wind flow angle changes from 0° to 90° or −90°, the ice mass augment firstly and then decreases. And for V-shape insulator strings with 60° - 120° inclination angle, the ice mass increases 47.22% in average compared to ordinary suspension insulators, which means that the insulators with wind flow angle (60° - 120°) are prone to ice disaster.
3) When $\alpha = \pm 40°$, the ice mass accretion on insulators is much more sensitive to the change of wind velocity compared to $\alpha = 0°$. When wind velocity increases, the increase rate of ice mass for insulator strings with $\pm 40°$ wind flow angle will become more and more lager than ordinary suspension insulator strings, which is significant to the evaluation of icing disasters for transmission lines.
4) In the design of insulator strings in icing regions, the effect of wind flow angle & velocity must be taken into consideration due to their significant effect on ice accretion. Otherwise, the transmission line will face the potential threat of ice over-load and icing flashover due to wrong prediction of ice mass.

REFERENCES

[1] M. Farzaneh and W. A. Chisholm, "Effects of ice and snow on the electrical performance of power network insulators," in *Atmospheric Icing of Power Networks*. Dordrecht, Holland: Springer, 2008, pp. 269–325.
[2] M. Farzaneh, "Insulator flashover under icing conditions," *IEEE Trans. Dielectr. Electr. Insul.*, vol. 21, no. 5, pp. 1997–2011, Oct. 2014.
[3] X. Jiang, L. Shu, and C. Sun, *Insulation of Electric Power System under Pollution and Icing Conditions*, (in Chinese). Beijing, China: China Electric Power Press, 2009.

[4] S. Berlijn, I. Gutman, K. Halsan, M. Eilertsten, and I. Gu, "Laboratory tests and Web based surveillance to determine the Ice- and snow performance of insulators," *IEEE Trans. Dielectr. Electr. Insul.*, vol. 14, no. 6, pp. 1373–1380, Dec. 2007.
[5] Q. Hu, L. Shu, X. Jiang, C. Sun, Z. Zhang, and J. Hu, "Effects of shed configuration on AC flashover performance of ice-covered composite long-rod insulators," *IEEE Trans. Dielectrics Electr. Insul.*, vol. 19, no. 1, pp. 200–208, Feb. 2012.
[6] Y. Liu, S. Gao, D. Huang, T. Yao, X. Wu, Y. Hu, and W. Cai, "Icing flashover characteristics and discharge process of 500 kV AC transmission line suspension insulator strings," *IEEE Trans. Dielectr. Electr. Insul.*, vol. 17, no. 2, pp. 434–442, Apr. 2010.
[7] Z. Vuckvic and Z. Zdravkovic, "Effect of polluted snow and ice accretions on high-voltage transmission line insulators," in *Proc. 5th Int. Workshop Atmos. Icing Struct.*, Tokyo, Japan, 1990, pp. 1–6.
[8] Y. Hu, X. Jiang, L. Shu, Z. Zhang, Q. Hu, and J. Hu, "DC flashover performance of ice-covered insulators under complex ambient conditions," *IET Gener., Transmiss. Distrib.*, vol. 10, no. 10, pp. 2504–2511, Jul. 2016.
[9] J. Zhang and M. Farzaneh, "Propagation of AC and DC arcs on icesurfaces," *IEEE Trans. Dielectr. Electr. Insul.*, vol. 7, no. 2, pp. 269–276, Apr. 2000.
[10] W. J. Rudzinski, M. Farzaneh, and E. P. Lozowski, "3D numerical and laboratory simulations of glaze ice accretion on a non-energized station post insulator," in *Proc. 11th Int. Workshop Atmospheric Icing Struct.*, Montréal, QC, Canada, 2005, pp. 1–9.
[11] Z. Zhang, X. Jiang, C. Sun, J. Hu, H. Huang, and D. Gao, "Influence of insulator string positioning on AC icing flashover performance," *IEEE Trans. Dielectr. Electr. Insul.*, vol. 19, no. 4, pp. 1335–1343, Aug. 2012.
[12] J. Xingliang, W. Quanlin, Z. Zhijin, S. Lichun, H. Jianlin, H. Qin, P. Yang, and C. Yi, "Estimation of rime icing weight on composite insulator and analysis of shed configuration," *IET Gener., Transmiss. Distrib.*, vol. 12, no. 3, pp. 650–660, Feb. 2018.
[13] X. Jiang, X. Han, Y. Hu, and Z. Yang, "Model for ice wet growth on composite insulator and its experimental validation," *IET Gener., Transmiss. Distrib.*, vol. 12, no. 3, pp. 556–563, Feb. 2018.
[14] *Compact Overhead Transmission Line Design Specification*, document China E S O S. Q/GDW110-2003, 2003.
[15] *220-500 kV Compact Overhead Transmission Line Design Specification*, document China I S O. DL/T5217-2005, 2005.
[16] S. Dingshen, C. Wei, and W. Jin, "Investigation on application of composite insulator for V-string," *Insulators Sure Arresters*, vol. 15, no. 201, pp. 14–16, 2004.
[17] Y. Bo, H. Lei, and W. Liming, "Study on loading characteristics of V-shape composite insulator used in 330 kV compact line," *Proc. CSEE*, vol. 15, no. 25, pp. 91–95, 2005.
[18] L. Hou, L. Wang, and Z. Guan, "Dynamics characteristic of V-string composite insulators for 330kV overhead transmission line," in *Proc. IEEE Conf. Electr. Insul. Dielectr. Phenomena*, Victoria, BC, Canada, Oct. 2006, pp. 429–432.
[19] Y. Liao, L. Hou, L. Wang, Z. Guan, Y. Zhang, and P. Zhu, "Included angle selection of V-Shape insulator string for 750-kV compact transmission line," *IEEE Trans. Power Del.*, vol. 26, no. 1, pp. 385–393, Jan. 2011.
[20] X. Jiang, Z. Xiang, Z. Zhang, J. Hu, Q. Hu, and L. Shu, "Predictive model for equivalent ice thickness load on overhead transmission lines based on measured insulator string deviations," *IEEE Trans. Power Del.*, vol. 29, no. 4, pp. 1659–1665, Aug. 2014.
[21] J. Y. Jin and M. S. Virk, "Study of ice accretion and icing effects on aerodynamic characteristics of DU96 wind turbine blade profile," *Cold Regions Sci. Technol.*, vol. 160, pp. 119–127, Apr. 2019.
[22] *User Manual of FENSAP-ICE*, FENSAP, Canonsburg, PA, USA, 2014.
[23] H. Beaugendre, F. Morency, and W. G. Habashi, "FENSAP-ICE's three-dimensional in-flight ice accretion module: ICE3D," *J. Aircr.*, vol. 40, no. 2, pp. 239–247, Mar. 2003.
[24] L. Makkonen, "Modeling of ice accretion on wires," *J. Climate Appl. Meteorol.*, vol. 23, no. 6, pp. 929–939, Jun. 1984.
[25] L. Makkonen, "Heat transfer and icing of a rough cylinder," *Cold Regions Sci. Technol.*, vol. 10, pp. 105–106, Feb. 1985.
[26] M. Farzaneh *et al.*, "Insulator icing test methods and procedures a position paper prepared by the IEEE task force on insulator icing test methods," *IEEE Trans. Power Del.*, vol. 18, no. 4, pp. 1503–1515, Oct. 2003.
[27] *Guide For Test Methods and Procedures to Evaluate the Electrical Performance of Insulators in Freezing Conditions*, IEEE Standard 1783, Oct. 2009.

YAFEI HUANG was born in Hunan, China, in June 1994. He received the B.S. degree in electric engineering from Chongqing University, China, in 2016, where he is currently pursuing the Ph.D. degree with the College of Electric Engineering. His research interests include icing disaster prevention of power grid, CFD-based ice simulation, and the design of high-voltage transmission line.

MUHAMMAD S. VIRK received the bachelor's degree in aerospace engineering from NUST, Pakistan, and the master's degree in aerospace engineering and the Ph.D. degree in computational fluid dynamics from U.K., in 2009. He is currently a Professor of cold climate technology with the University of Tromsø (UiT), Norway. At UiT, he established the research activities and infrastructure related to atmospheric icing, cold climate technology, computational fluid dynamics (CFD), and wind energy. With his experience of renewable energy and CFD based numerical modeling of complex turbulent flow behaviors and heat transfer, he is also having a good understanding of the aircraft design and aspects related to high speed aerodynamics from his aerospace engineering background. He is also leading the Arctic Technology & Icing Research Group, UiT. He is also the author of 140 scientific publications (peer-reviewed journal publications and international conference proceedings).

XINGLIANG JIANG (Senior Member, IEEE) was born in Hunan, China, in July 1961. He received the B.S. degree from Hunan University, and the M.S. and Ph.D. degrees from Chongqing University. He is currently working as a Professor with the College of Electric Engineering, Chongqing University. He is also the author of more than 200 scientific publications. His research interests include icing disaster prevention of transmission line, CFD based ice simulation, online monitoring of power grid, and the design of high-voltage transmission lines.